catalysts

MDPI

Article

Benefit of LDH-Derived Mixed Oxides for the Co-Oxidation of Toluene and CO Exhausted from Biomass Combustion

Caroline Paris, Hadi Dib, Charf Eddine Bounoukta *, Eric Genty, Christophe Poupin, Stéphane Siffert and Renaud Cousin *

U.R. 4492, UCEiV, Unité de Chimie Environnementale et Interactions sur le Vivant, Université du Littoral Côte d'Opale, F-59140 Dunkerque, France; caroline.paris@univ-littoral.fr (C.P.)
* Correspondence: charf-eddine.bounoukta@univ-littoral.fr (C.E.B.); renaud.cousin@univ-littoral.fr (R.C.)

Abstract: The proposed study is devoted to highlighting the importance of mixed oxides preparation through the layered double hydroxide route for undesirable gas pollutants abatement. Different series of Cu/Al/Ce mixed oxides with similar or different stoichiometrics were prepared and compared for toluene and/or CO oxidation. Catalyst synthesis methods influence material properties and activity for oxidation reactions. The high activity for the oxidation reactions of mixed oxides derived from LDH is explained by the Cu/Ce synergy. The presence of CO in the CO/toluene mixture does not affect the total toluene oxidation, and the toluene does not affect the total oxidation of CO conversion at low temperatures. The most effective catalytic material ($Cu_6Al_{1.2}Ce_{0.8}$) presents a long lifetime stability for total toluene oxidation and resistance to CO poisoning in mixtures.

Keywords: copper oxide; cerium oxide; LDH; mixed metal oxides; toluene; CO; co-oxidation

Citation: Paris, C.; Dib, H.; Bounoukta, C.E.; Genty, E.; Poupin, C.; Siffert, S.; Cousin, R. Benefit of LDH-Derived Mixed Oxides for the Co-Oxidation of Toluene and CO Exhausted from Biomass Combustion. *Catalysts* **2024**, *14*, 455. https://doi.org/10.3390/catal14070455

Academic Editors: Ioan-Cezar Marcu and Octavian Pavel

Received: 7 June 2024
Revised: 11 July 2024
Accepted: 11 July 2024
Published: 16 July 2024

1. Introduction

During the last decade, increasing interest has been directed towards the research of environmental pollution control and fossil fuel replacements for domestic heating using biomass as an alternative resource [1–3]. Organic raw feedstocks with low costs, WORLDWILD availability and suitability of use are ideal candidates and considered as a tool and technology for fulfilling the goals of carbon neutrality, preventing climate change and bioresource use [4]. However, the use of biomass as fuel during combustion can generate a mixture of pollutants containing several molecules of different types: CO, Volatile Organic Compounds (VOCs) and NOx, with various concentrations [5–8]. Thus, the emissions from non-efficient biomass combustion can be higher than those from fossil fuel burning [9]. The exhausted effluents address, in the presence of hazardous substances with different proportions in the environment, problems associated with healthiness while additionally having a negative impact on the greenhouse effect [10]. Particularly, CO and toluene are well known as highly toxic and seriously harmful to human health.

The catalytic oxidation of CO and toluene is a highly desirable solution [11–14]. The pollutants will be converted directly to harmless gases with a simple process and at relatively low temperatures [15]. Nevertheless, highly efficient, low-cost and environmentally friendly catalysts remain ambiguous. Toluene oxidation involves abundant intermediates with strong chemical activity and hence the rapid total degradation of CO_2 and H_2O with no release of side products, which are pollutants to the environment [16]. Oxidation with solid catalytic materials is a well-studied and industrially useful process [17–19]. The majority of heterogeneous catalysts employed for the pollutant remediation are based on Pt and Pd noble metals [20]. However, from an economic perspective, the high-priced catalysts make their industrial application challenging. Low-cost mixed metal oxides containing Co, Cu, Al and Mn or lanthanide metals with good catalytic performance and stability can offer an opportunity to carry out VOCs and CO oxidation at optimum reaction conditions [21–30].

Recently a significant achievement has been made in the catalytic oxidation of toluene and CO by copper- and cerium-based mixed oxides [31–36]. Nevertheless, it is still a challenge to adjust different frameworks to fully understand the reaction process and catalytically oxidize toluene and CO with high efficiency. Few studies have been published on the heterogeneous catalysis oxidation of toluene in the presence of others [37]. The reaction behavior and mechanism are probably quite different from those of the catalytic oxidation of individual pollutants. For instance, S. Mo et al. [38] found that toluene oxidation was improved in the presence of CO with Co_3O_4-based catalysts in contrast to Pt/Al_2O_3. Unfortunately, CO transformation over used catalysts was inhibited significantly by toluene, even though the reaction oxidation mechanism of both molecules was not affected. The same group studied a series of Pt-based supported metal oxide catalysts. One can prove that using CeO_2 support effectively alleviates the mutual inhibition between CO and toluene oxidation. The research paper describes the importance of oxygen storage in catalysts for the competitive adsorption of both molecules and, consequently, for enhancing the catalytic activity. Additionally, F. Bi et al. [39] found that when using non-oxide C_3N_4-supported Pd or Pt, the catalytic efficiency of CO was inhibited in the presence of mixed components. Furthermore, in S. B. Kang's publication works [40,41], the CO poisoning effect on multi-VOCs (including toluene) over bimetallic Pd/Pt-supported alumina powders and monoliths was explored. The authors claimed that CO inhibition can be controlled by engineered monolith catalysts, where the metal ratio and the design of multiple zone systems were considered.

However, using a non-noble metal could be an interesting method. Indeed, in our previous studies, mixed oxides derived from a Layered Double Hydroxide (LDH) structure (denominated as Mg/Al/Ce and Co/Al/Ce) were tested for the toluene oxidation in the presence of CO [42,43]. These studies revealed an improvement in the toluene oxidation activity performance when toluene was in a mixture with other pollutants. It can be clearly observed that the reaction intermediates presented are quickly different from single to mixture reaction oxidation. Nonetheless, the catalytic CO oxidation in the presence of the mixture was not discussed.

It is therefore clear that proposing and developing more efficient catalysts and understanding the active sites on toluene and CO mixture oxidation are of fundamental importance. The present work approaches some degree of VOCs abatement in real conditions. The study reports different preparation methods of mixed oxide catalysts for toluene/CO simple or mixture oxidations. Mixed oxides with a metal molar ratio of Cu/Al/Ce of 6/1.2/0.8 with different textural and structural properties were synthetized and used in the same conditions. Their characterization and catalytic activity were investigated. Furthermore, the effect of Ce ratio loading on the mixed oxide structure-derived LDH was evaluated and optimized. In addition, the effect of the CO concentration on the mixture feed and, finally, the catalyst reuse was considered.

Thus, the novelty of this work is it exemplifying that preparing mixed oxides via the layered double hydroxide method is a promising strategy for developing robust, stable catalysts without noble metals to treat pollutants (VOCs and CO) issued from wood combustion.

2. Results and Discussions

The analytical section (Section 3) covers the preparation method and nomenclature of the studied materials.

2.1. Catalysts' Characterization

The catalysts' structural parameter values obtained by ICP are listed in Table S1 of the Supplementary Materials and showed the same nominal proportion of metal in the ternary oxides. X-ray patterns of the prepared mixed oxides and JPCDS cards of their plausible corresponding phases are shown, respectively, in Figure 1 and Figure S1. CuO and CeO_2 diffractograms showed that single metal-containing samples are found, respectively, as an oxide phase with XRD reflections corresponding to the pure monoclinic CuO (JCPDS

card N°48-1584) and pure cubic CeO_2 (JCPDS card N°34-0394). A copper oxide phase appears for all the mixed oxides; the samples reveal the presence of CuO plane families with similar forms to that of the single metal oxide. The same goes for the Ce; when it is present, catalysts displayed several diffraction patterns corresponding to the CeO_2 structure. For the mechanically mixed pure metal oxides, the structure of the α-Al_2O_3 (JCPDS card N°46-1212) phase with a rhombohedral form was evidenced. Unfortunately, the Al diffractions were absconded for other catalysts, even though the element was loaded in the mixed oxide's structure. This is mainly due to the high dispersion with a low average size or the Al element being in an amorphous form. Indeed, a close inspection of the mixed oxides derived from the LDH pics reveals q low intensity, which suggests that crystallites are divided nearby.

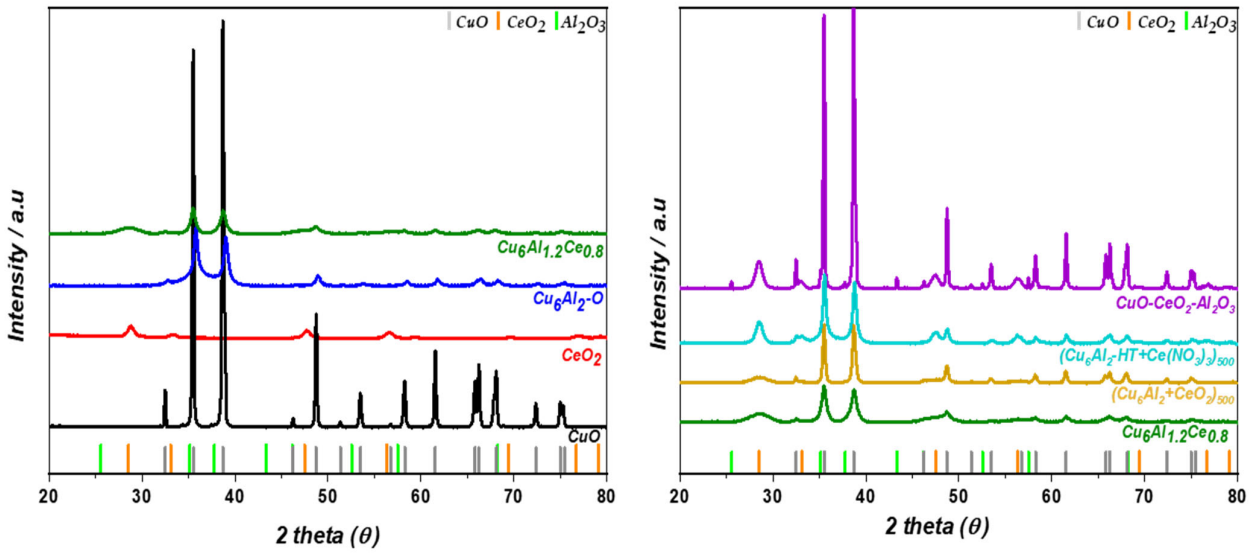

Figure 1. XRD patterns of the prepared oxide catalysts.

Table 1 summarizes the calculated average crystallite size of both the CeO_2 and CuO phases. The XRD analysis of CuO powder indicated the presence of bulky nanocrystals or even suggested the presence of large CuO monocrystals. In contrast, the CeO_2 phase ratifies the presence of crystallite with less than 10 nm for all samples. The detected values for the LDH-derived metal oxides structure for CuO range between 15 and 21 nm, while the CeO_2 was around 3–4 nm. The size of both phases for the CuO-Al_2O_3-CeO_2 sample remain unchanged after the mechanical mixing of the three pure metal oxides. The cubic crystallite size was unaffected when ceria was mixed with the Cu_6Al_2 sample, but the CuO phase became slightly smaller. Copper's presence in the LDH skeleton before calcination ensures the formation of a lower crystal size, with the presence of Ce becoming lower. Thus, a small crystallite size of these phases was observed for the $Cu_6Al_{1.2}Ce_{0.8}$ catalyst.

The textural properties of the mixed oxides were investigated in terms of the BET-specific area (Table 1). The prepared single-metal oxide CeO_2 presented high values (95 m^2/g), in contrast to the as-received CuO oxide calcined powder (14 m^2/g). Similar to the structural parameters, CuO-Al_2O_3-CeO_2 have the same textural properties as the raw copper oxide. The specific surface area of the other mixed oxides ranges between the corresponding parameters of the pure metal oxide. Cerium's presence in the sample increases the measured BET surface, and then $Cu_6Al_{1.2}Ce_{0.8}$ texture was two times higher compared to that of other mixed oxides. The porosity of the calcined LDH is ensured by the interlamellar space of the precursor. Moreover, in mixed oxides, the nearby separate aggregates of both crystallites with lower sizes permit the formation of a rich abundant-pores surface.

Table 1. Calculated structural and textural parameters of the prepared metal oxides.

Sample	Crystallite Size (nm)		BET Surface Area (m^2/g)
	CuO	CeO_2	
CuO	44.4	-	14
CeO_2	-	9.0	95
Cu_6A_{l2}	17.0	-	17
$Cu_6Al_{1.2}Ce_{0.8}$	15.2	3.3	47
$CuO\text{-}Al_2O_3\text{-}CeO_2$	44.0	9.4	14
$(Cu_6A_{l2}\text{-HT} + Ce(NO_3)_3)500$	25.1	9.4	27
$(Cu_6A_{l2} + CeO_2)500$	21.0	4.0	25

H_2-TPR analysis was used to determine the reducing capability of the catalysts (Figure 2). Ceria reduction was not observed above 500 °C. Pure CuO with bulky crystallites present one broad region with a maximum temperature T_{max} = 320 °C, corresponding to the reduction of the Cu^{2+} cation to Cu(0) [44] The same characteristic peak in this region appears in the case of $CuO\text{-}Al_2O_3\text{-}CeO_2$ mixed oxides but at lower T_{max} values with a higher consumption of hydrogen. Therefore, the direct physical mixing of metal oxide powders provides a negligible synergetic interaction between the presented metals.

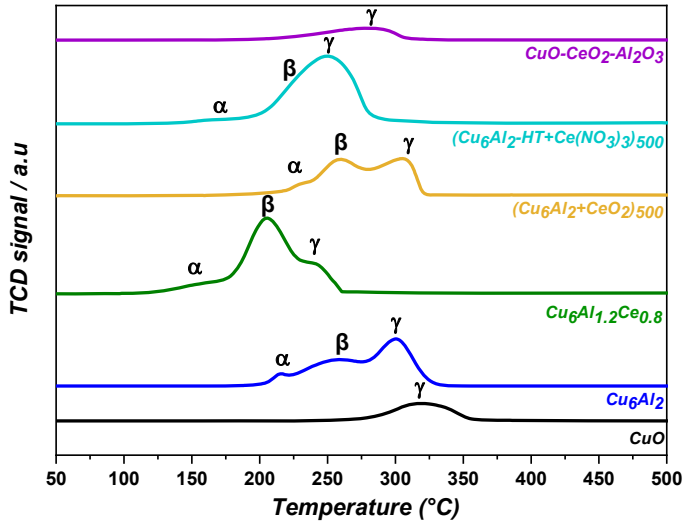

Figure 2. H_2-TPR profile of the prepared oxide catalysts.

The H_2-TPR profile for the other samples was deconvoluted into three regions, α, β and γ [45], using Gaussian fitting. The peak α is assigned to the interfacial strongly interacted copper with ceria or even the nearby aluminum issued from the oxidation of the LDH skeleton [46]. The second T_{max} peak appearing at a temperature range of 200 to 260 °C is most probably due to the reduction in separate CuO crystallites with a low average size. The α and β are assigned directly to the lattice vacant and mobile oxygen species. The third peak is associated with the bulky CuO clusters that are hardly reduced. The summit's position and H_2 consumption (Table S2) change with the mixed oxides preparation method. The high-temperature positions of two peaks of the $(Cu_6Al_2 + CeO_2)_{500}$ are similar to that of their primary precursor Cu_6Al_2; however the lowest onset reduction temperature was extended, and the hydrogen consumption region was greater.

Mixing a cerium nitrate precursor with the LDH structure (Cu_6Al_2-HT) before oxidation generally downgraded the T_{max} of the mixed oxide. Nonetheless, the hydrogen consumption of the third region was still high due to the big crystallite size obtained with this sample. In contrast to others, the $Cu_6Al_{1.2}Ce_{0.8}$ T_{max} of the three-reduction peaks was significantly inferior, which indicates a huge reducibility character. A high consumption of

H_2 was depicted for the α, β position, contrary to the γ part, where the hydrogen uptakes were at the bottom. With this sample, the redox properties are stronger and the reduction in the scarceness of the bulky crystallite is easier [47].

The amount of copper and the textural properties of the catalysts are other factors that may influence the reducibility of the catalyst. The H_2 consumption in the γ region was increased in the opposite direction to the T_{max} from single to ternary oxides. This is directly related to the reduced copper content associated with the increased specific surface area.

The catalyst's characterization spotlights the influence of the preparation method and the Ce loading on the textural–structural properties of the mixed oxides. LDH structure precursors for mixed oxides preparation present highly well dispersed copper oxide. Moreover, Ce's presence, in general, lowers the CuO average crystallite size and induces a new couple redox. The interfacial one is assured by the presence of the metal on the LDH skeletons before oxidation. Nearby Ce^{4+} and Cu^{2+} from the LDH calcination interface substitution had the same ionic radii and then improved the lattice oxygen vacancy [48].

2.2. Catalytic Tests

2.2.1. Individual Toluene Oxidation

The light-off curves of total toluene oxidation that present the conversion as a function of the temperature are shown in Figure 3. In general, the carbon balance for toluene conversion during all experiments was superior to 85%. The detected reaction products were CO_2 and H_2O, as well as traces of CO and benzene at a low conversion. No reaction intermediates are detected; small molecules are oxidized rapidly and are barely accumulated within the catalyst surface before the transformation to CO_2 and H_2O.

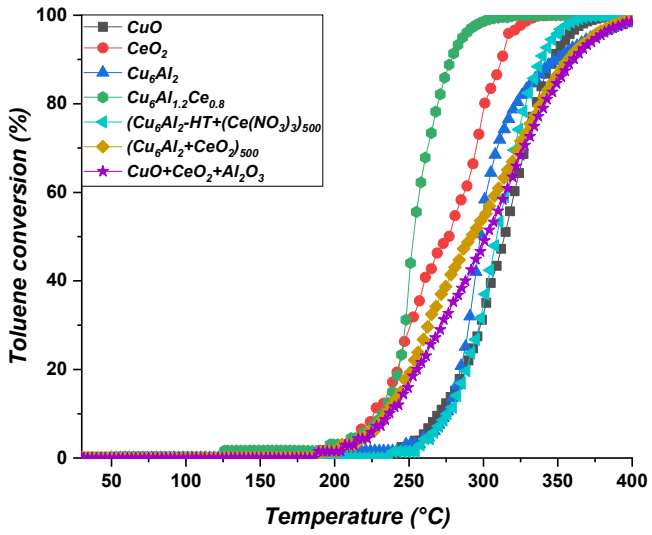

Figure 3. Light-off curves for toluene oxidation over oxide catalysts.

Toluene conversion under air was affected by the type of metal oxides used. The detailed data for 10, 50 and 90% toluene conversion are listed in Table S3. The T_{50} (temperature corresponding to 50% of the conversion) of the toluene results indicated that CuO is the less active catalyst, among others. In the presence of Ce, the T_{50} over prepared oxides shifted to a lower temperature by the presence of a new induced redox couple. The Cu_6Al_2 activity is comparable to that for ternary oxides prepared by a mechanical mixture. The T_{50} is between 292 and 309 °C, while their corresponding T_{90}, in general, was higher than 320 °C.

Single-oxide ceria with a high specific area set out a good activity for toluene oxidation with T_{50} = 277 °C and T_{90} = 312 °C, respectively. However, the results are still far from those obtained by $Cu_6Al_{1.2}Ce_{0.8}$. An excellent activity was achieved by ternary mixed oxide derived from LDH with a T_{50} at ~254 °C and a T_{90} at ~277 °C.

At higher temperatures the pure CuO ranks better than some mixed metal oxides. At high temperatures, the bulky CuO becomes active, but this can be expected for the sintering of highly separate, small CuO crystallites presented on the mechanically synthetized mixed oxides CuO-Al_2O_3-CeO_2.

In combination with the catalytic and characterization results, an increase in the specific surface area leads to an upward catalytic activity (Table 1). The higher surface leads to towering high oxygen storage, and consequently, more toluene transformation occurs. Such behavior is explained by the high activity of single ceria and $Cu_6Al_{1.2}Ce_{0.8}$ catalysts. The comparison results showed that mixed oxides samples cover the highest reducibility at low temperatures by interfacial oxygen vacancies, and the small crystallite size of copper oxide/cerium oxide with a good specific surface can monitor toluene oxidation easily.

2.2.2. Individual CO Oxidation

As for CO oxidation, which is directly transformed to CO_2, $Cu_6Al_{1.2}Ce_{0.8}$ still shows the best performance on individual molecule abatement, but this time at real low-grade temperatures (Figure 4).

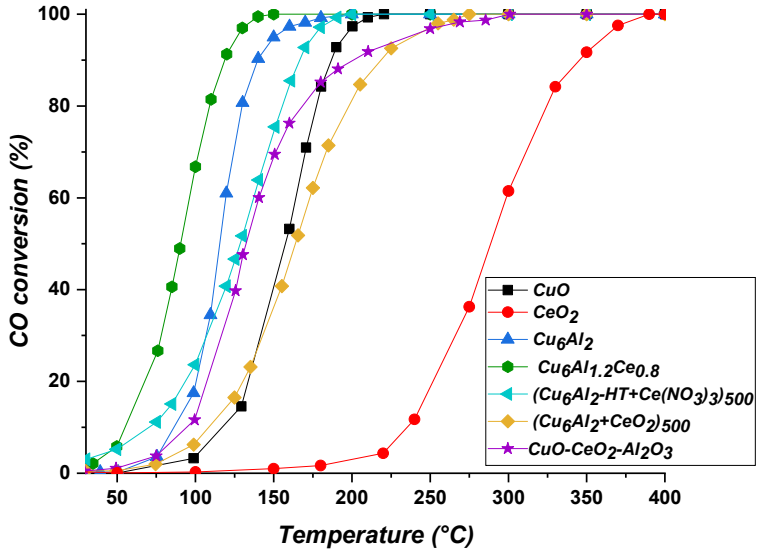

Figure 4. Light-off curves for CO oxidation over oxide catalysts.

The T_{50} and T_{90} values were reduced, respectively, from 254 and 277 °C for single toluene oxidation to 91 and 119 °C for single CO oxidation (Table S4). Outbidding oxidation performances for CeO_2 were totally decreased, and the catalyst reached no more than 20% CO conversion at T = 250 °C. The activity order for other catalysts also changed. Calcined commercial CuO powders reached 50% CO conversion before the $(Cu_6Al_2 + CeO_2)_{500}$ catalyst, and the T_{90} was significantly less than that of both the mentioned and CuO-CeO_2-Al_2O_3 mixed oxides. $(Cu_6Al_2$-HT + $Ce(NO_3)_3)_{500}$ ranked third for CO total oxidation, and this likewise true for toluene. The CO oxidation rate is much higher for the $Cu_6Al_{1.2}Ce_{0.8}$ catalyst sample, followed by Cu_6Al_2, where the Ce is not present.

Herein, CO conversion to CO_2 occurred at distinct active sites regarding toluene, and the $Cu_6Al_{1.2}Ce_{0.8}$ sample exhibited particular crucial sites that are available in oxidizing both molecules with enhanced efficiency. It seems that CuO is the active phase for CO oxidation with regard to ceria and the raw binary metal oxides Cu_6Al_2 activities.

From the results, the most likely factor for CO transformation over mixed oxides is that the low crystallite size of CuO can be easily reduced, and therefore, the activity of CO oxidation is much higher.

Catalytic oxidation is related to the redox properties and structural–textural parameters. The redox couples in our catalysts are the Ce^{4+}/Ce^{3+}, Cu^{2+}/Cu^{+} and Cu^{+} species results of the interfacial redox interactions between the CuO and CeO_2 phases [49]. It is

suggested that, in the case of toluene oxidation, the three mentioned couples are active, and they have the same potential for oxidation reactions. However, it is accepted that the CO mechanism occurs mostly by the Mars–van Krevelen reaction mechanism over the Cu-based catalyst, in which Cu undergoes oxidation and reduction reactions via the oxygen vacancy lattice [50].

Thus, CO oxidation needs a catalyst reoxidation scope, given by both the surface oxygen exchange ability and oxygen mobility. Meanwhile, toluene oxidation indicates that just the oxygen swap capacity is sufficient. However, as the Cu/Ce synergistic effect accelerates the redox cycling rate for CO transformation, it could also improve the overall toluene oxidation by increasing the free energy adsorption of the reaction intermediates, facilitating rapid CO_2 production from the aromatic molecule.

The catalytic efficiency highlights once more the importance of the LDH route for CuCeAl mixed oxides preparation. With $Cu_6Al_{1.2}Ce_8$, toluene or CO molecules could be directly oxidized by adjacent active oxygens around the CuO/CeO_2 interfacial sites, and gaseous oxygen was then quickly captured and dissociated to continuously produce new active oxygen species. Also, satisficing the specific surface area leads to an increase in the defect site concentration, and therefore, the oxidation dispatch was improved.

2.2.3. Toluene and CO Co-Oxidation

The catalytic exhaustion of a toluene and CO gas mixture by oxidation over the prepared mixed oxides was investigated, and the tests results are shown in Figure 5. The T_{50} of toluene (Table S5) for both single-metal oxides (CuO, CeO_2) were displaced to higher temperatures by 10–13 °C.

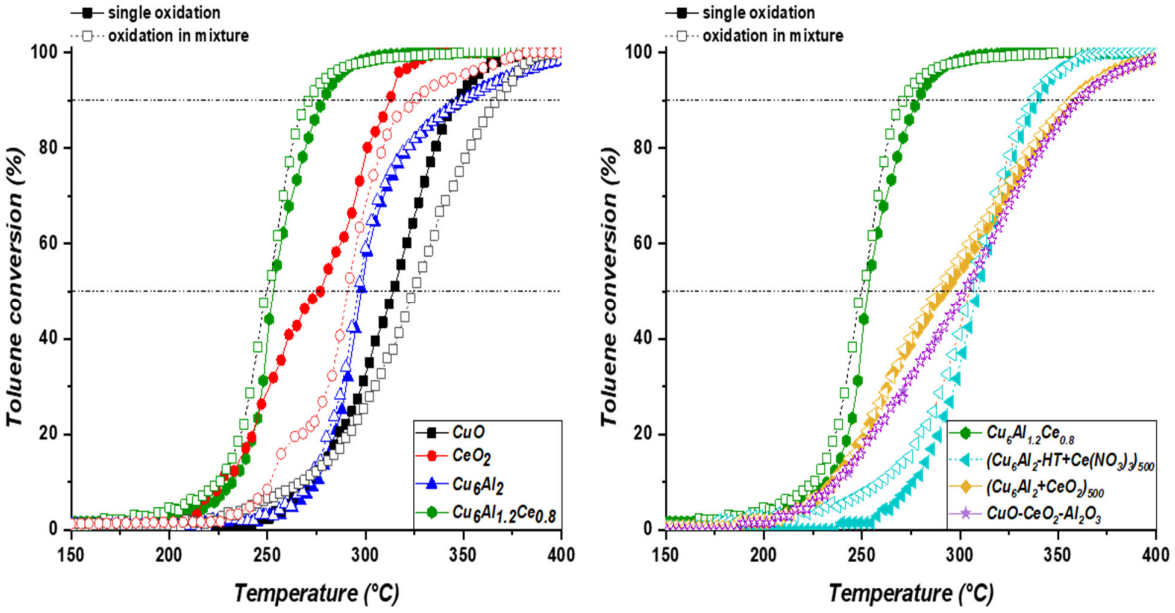

Figure 5. Light-off curves for toluene conversion in simple and mixture feed over oxide catalysts (solid line: single toluene oxidation; dashed line: in the presence of CO).

The worst CuO sample activity drops down more in the mixture, and CeO_2 catalytic behaviors becomes quasi-similar to the mechanically mixed solids. Mixed oxides show similar scenarios as the individual toluene oxidation, with a maximum shift to a lower temperature of 4 °C. This can indicate that CO did not inhibit the toluene oxidation, in contrast to some previously examined supported noble metal catalysts [37,39]. The $Cu_6Al_{1.2}Ce_{0.8}$ sample still led and achieved 50% conversion at a slightly lower temperature compared to when it was singly oxidized. The low-temperature moderate toluene conversion by the mixed oxide in a mixture is mainly due to some change in the oxidation mechanism and the presence of suitable and available active sites for converting toluene in the presence of

CO. Also, it is suggested that toluene transformation to intermediates can be processed by the produced CO_2 or even CO [51,52].

On the other hand, all Cu-based catalysts reach total CO oxidation in the mixture before toluene (Figure 6). The unfunctionalized aromatic molecules adsorb relatively weakly on the mixed oxides regarding the CO. Exclusively for the $Cu_6Al_{1.2}Ce_{0.8}$ sample, CO oxidation performances in the mixture at conversion values inferior than 50% were significantly decreased, with small alterations in the catalytic order. Ternary mixed oxides rank better than Cu_6Al_2. However, despite being active and still reaching a high total CO oxidation before others, the $Cu_6Al_{1.2}Ce_{0.8}$ tendency for total CO conversion during the oxidation of a mixture was decreased compared to that observed for single oxidation. At low temperatures, the oxygen reaction with toluene exerted a high exothermicity character that would increase the local temperature on the catalyst surface, improving the CO transformation at temperatures below 115 °C. Nevertheless, the curve allure for $Cu_6Al_{1.2}Ce_{0.8}$ displayed a steady state at a temperature range of 115–166 °C for CO oxidation in the mixture. This is the well-known poisoning effects of second components on VOCs abatement relative to competitive adsorption [53]. This is likely due to the fact that non-reacted adsorbed bulky toluene molecules barely accumulated on the surface of the catalyst, reducing the available oxygen and the redox cycle rate. Therefore, the reaction entered the slowest step until the intermediate products of toluene were completely converted to small molecules and then oxides together with CO and CO_2 and, finally, gaseous oxygen replenished the active oxygen consumed in the reaction process.

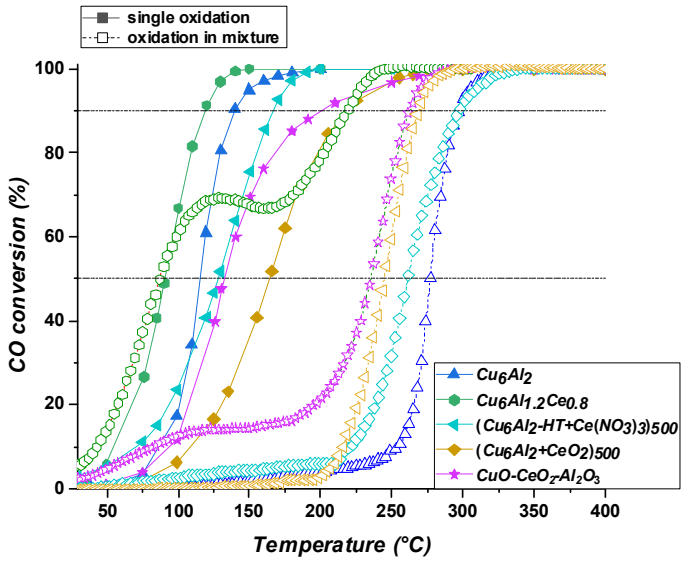

Figure 6. Light-off curves for CO conversion in simple and mixture feed over oxide catalysts (solid line: single CO oxidation; dashed line: in the presence of toluene).

It was demonstrated by several in situ insights that toluene and CO oxidation intermediates are bicarbonate bidentate with the active sites before CO_2 formation [53–55]. At the moment, when the temperature conditions favor high reactive adsorption, the active sites will be saturated and prevent a redox cycle. By increasing the temperature, CO_2 forms easily and the CO transformation process can be further promoted.

However, the T_{50} of CO oxidation in the presence of toluene for the $Cu_6Al_{1.2}Ce_{0.8}$ catalyst is much lower than the ones obtained over recently studied catalysts [37–39,56].

2.2.4. Influence of the Ce Fraction on the $CuAl_{2-x}Ce_x$ Structure for Toluene and CO Co-Oxidation

The cerium proportion of the mixed oxides has a crucial impact on the catalytic performances of CO and VOCs abatement. In this sense, the influence of the Ce ratio loading on the $Cu_6Al_{2-x}Ce_x$ (x = 0, 0.2, 0.4, 0.6, 0.8) structure prepared through the LDH

method for the toluene/CO mixture co-oxidation was studied. From Figure 7 with respect to the Cu_6Al_2 sample, all the series comply with the same order for single toluene and CO oxidation. In general, whatever the catalyst, T_{50} values for toluene conversion in the mixture are consistent with those of simple feed (Table S6). $Cu_6Al_{1.2}Ce_{0.8}$ and $Cu_6Al_{1\cdot4}Ce_{0\cdot6}$ catalysts exhibit the highest catalytic activity (T_{50} = 220 °C), while such decreases for the Ce fraction could slow down the oxidation process. The increase in the Ce content causes more amorphosity by promoting the presence of more defects. This is reflected by the decrease in the average pore size while the specific area and the total pore volume are increased (Table S7).

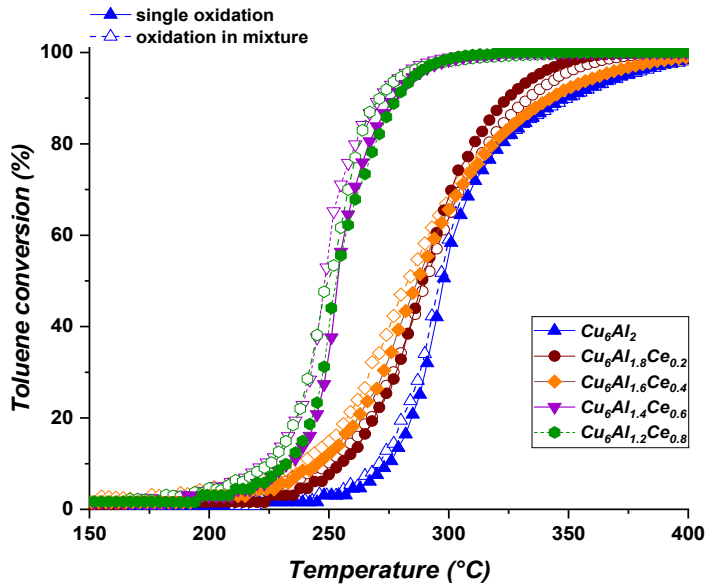

Figure 7. Light-off curves for toluene conversion in simple and mixture feed over $Cu_6Al_{2-x}Ce_x$ (x = 0–0.8) catalysts (solid line: individual toluene oxidation; dashed line: in the presence of CO).

Here, this amorphosity of the materials could be used to induce more reactive coverage and more efficient reducibility, as can be seen by TPR (Figure 8).

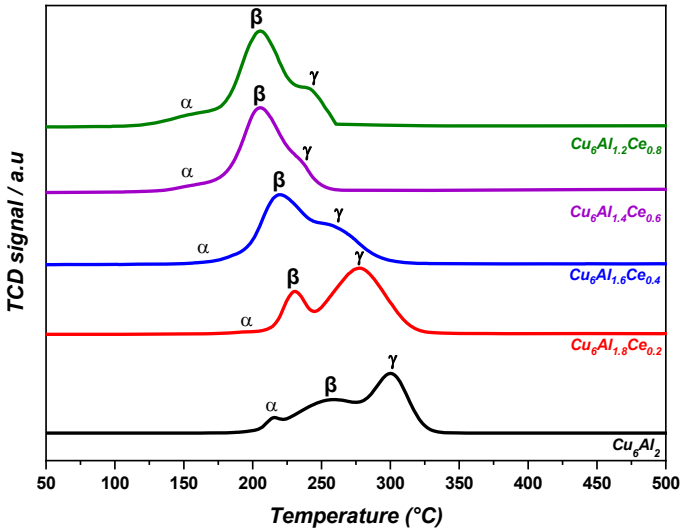

Figure 8. H_2-TPR profile of $Cu_6Al_{2-x}Ce_x$ catalyst series.

However, at some point, further Ce loading allows for maintaining stability or slightly declining the toluene catalytic oxidation by extensively reducing the copper content, negatively affecting the same parameters. The Cu content decreases with increasing Ce on the

catalyst. Nevertheless, the further loading of Ce from 0.6 to 0.8 allows for decreasing the specific surface area and the high hydrogen consumption in the β region. This is suggested by the presence of separate CeO_2 that decreases the number of oxygen vacancies related to the Cu/Ce interfacial surface.

Concerning the effect of the cerium content for the CO oxidation, Figure 9 illustrated that for the increase in CO_2 formation from single CO transformation, the higher reducibility at low temperatures is important. Meanwhile, CO oxidation in the mixture is more prone to inhibition by Cu/Ce interfacial oxygen poisoning.

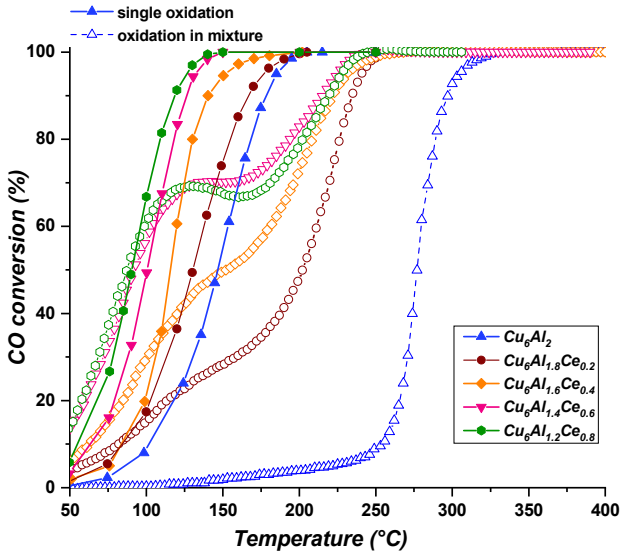

Figure 9. Light-off curves for CO conversion in simple and mixture feed over $Cu_6Al_{2-x}Ce_x$ (x = 0–0.8) catalysts (solid line: individual CO oxidation; dashed line: in the presence of toluene).

CO conversion was displaced to a higher temperature with a great detected shift for the Cu_6Al_2 sample. The ternary oxides ($Cu_6Al_{2-x}Ce_x$) reach total CO co-oxidation at approximately similar temperatures, although the catalytic performance at low temperatures is different and directly related to the reductive capacity at the peak position β, like toluene. Between 115 and 166 °C, the CO conversion rate begins to decrease. As the amount of cerium increases, it becomes more pronounced and weaker until the curve shows a stable pattern with cerium contents of 0.8 and 0.6. Therefore, the same interfacial oxygen vacancy lattice that participated for more activity was highly affected by strong CO poisoning. (Full $Cu_6Al_{2-x}Ce_x$ series characterization and detailed discussions have been reported in our previous study [57]).

2.2.5. CO Concentration Effect on the Toluene Oxidation in Mixture

Carbon monoxide is rottenly presented on the gas effluents and has a major impact on the oxidation efficiency. The co-oxidation of a mixture of different CO concentrations over our optimum catalyst does not affect the toluene transformation profile (Figure 10).

In general, at low temperatures, the mixture oxidation activity decreased with increasing CO concentrations. The CO conversion values at a temperature of 115 °C were diminished from 81% for 500 ppm CO to 55% for 2000 ppm. CO transformation is limited by the availability of active oxygen species. Interestingly, for a 1000 ppm concentration of CO, the conversion was slightly better in the mixture. The exothermic oxidation reaction of the mixture could induce the rapid conversion CO rate by the local surface temperature increasing. From another part, the steady region (115–166 °C) was affected by the same parameter where the CO rate decrease started to be more apparent. Without toluene, the empty surface-active sites have a scope for CO coverage and reaction rate promotion by the interfacial oxygen vacancy. However, when toluene is present and the total carbon

concentration in the stream increases, the available oxygen is limited and the interfacial redox cycle is slowed down.

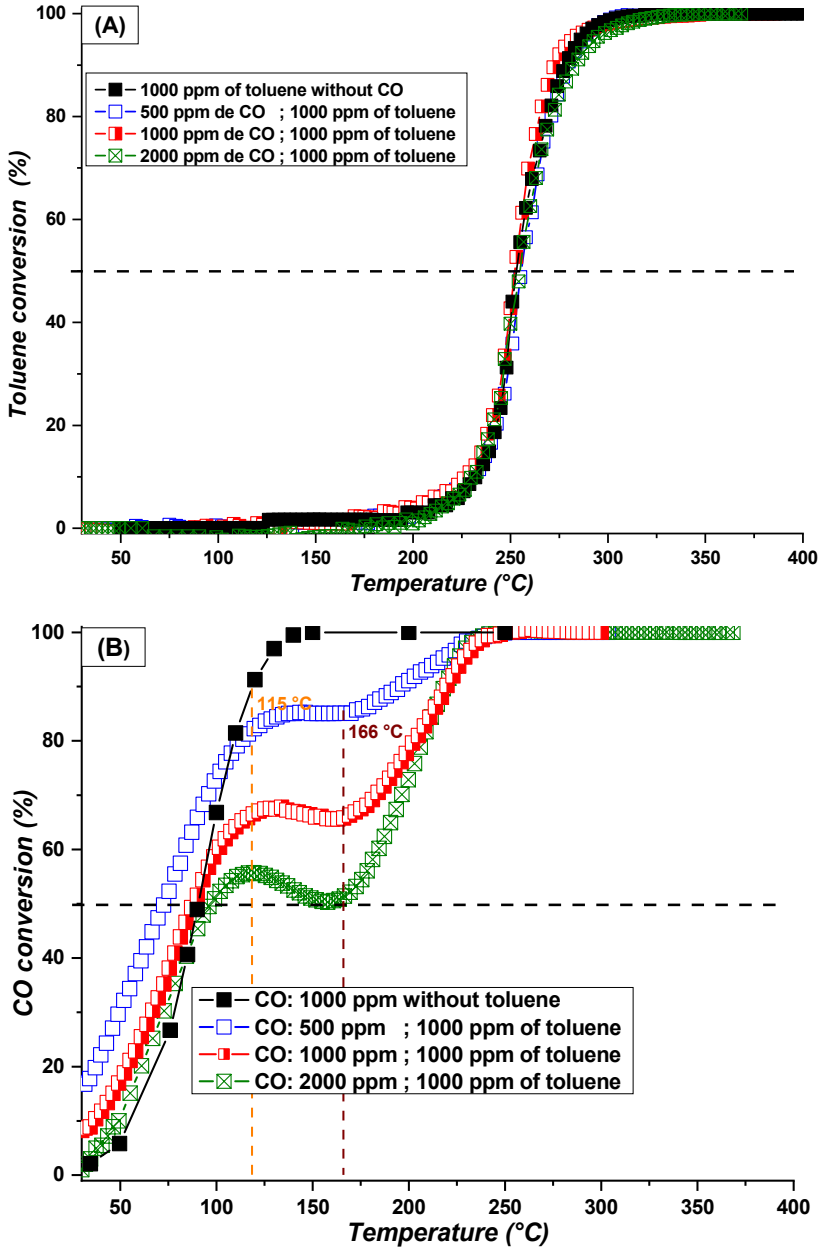

Figure 10. CO concentration effect on the toluene/CO mixture co-oxidation over the $Cu_6Al_{1.2}Ce_{0.8}$ mixed oxides catalyst. (**A**) Light-off curves for toluene conversion; (**B**) Light-off curves for CO conversion (solid line: individual toluene oxidation; dashed line: in the presence of CO).

2.2.6. Catalyst Reuse

The catalyst's stability was assessed by performing four consecutive light-off test cycles (Figure 11).

No significant change in the toluene oxidation was noticed with a 1000 ppm CO concentration in the mixture at lower temperatures. Nonetheless, a small drop-in at higher-temperature total toluene conversion followed by stable activity can be observed after the first cycle. It is therefore possible to reuse the catalyst after several heat treatments under toluene/CO flow. TGA-DSC is an useful tool for coke amount formation detection (Figure S2).

The characterization of the raw and used $Cu_6Al_{1.2}Ce_{0.8}$ sample with thermogravimetry analysis indicated that the presented physiosorbed water molecules after the reaction were hardly released, no carbon was deposited and no active sites leaching happened. This means that our catalyst should maintain its operation at a long duration after the first cycle without change and suggests that the slight loss of activity for the first time can tentatively be attributed to the further reduction of the Cu^{2+} small crystallite size to Cu metallic at higher temperatures.

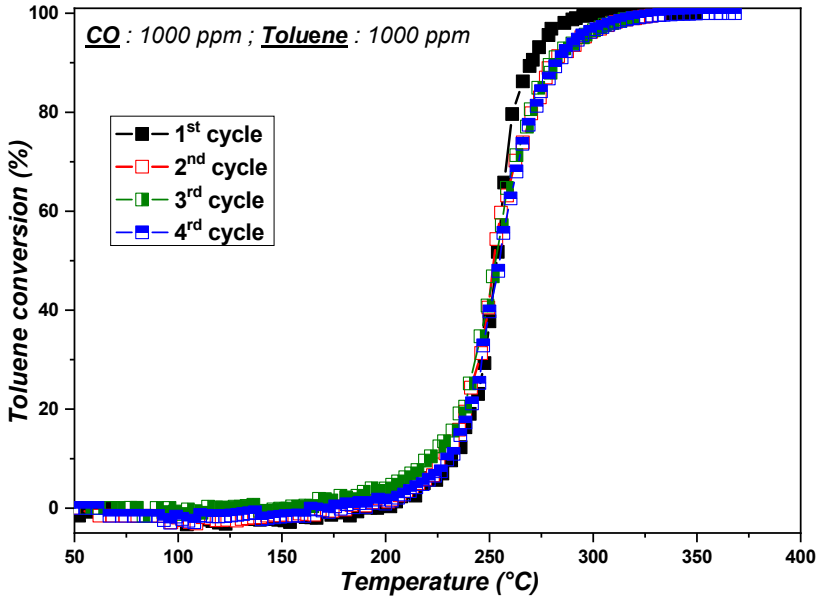

Figure 11. Catalyst reuse over the $Cu_6Al_{1.2}Ce_{0.8}$ mixed oxides catalyst. Reaction conditions: 1000 ppm of toluene, 2000 ppm of CO, 100 mg of the catalyst and 100 mL/min of total flow.

3. Analytic Section

3.1. Reagents

Copper nitrate trihydrate ($Cu(NO_3)_2$ $3H_2O$, 98%), aluminum nitrate nonahydrate ($Al(NO_3)_3$ $9H_2O$, 98.5%), cerium nitrate hexahydrate ($Ce(NO_3)_3$ $6H_2O$, 99.5%), sodium hydroxide (NaOH, 98%), sodium carbonate (Na_2CO_3, 99.5%), copper oxide (CuO, 100%), alumina (Al_2O_3, 100%) and toluene (C_7H_8, 100%) all purchased from Thermo Scientific Research (ThermoFisher Scientific, Illkirch, France), as well as carbon monoxide 1% CO/N_2 (Messer, Suresnes, France), were used for the chemical synthesis of materials or catalytic testing in the case of the last two named compounds.

3.2. Catalysts Preparation

A cerium hydroxide obtained by cerium nitrate hexahydrate precipitation in the presence of sodium hydroxide was calcined at 400 °C for 4 h using a 1 °C min^{-1} ramp under an air flow of 4 $L{\cdot}h^{-1}$ to finally obtain the pure cerium oxide (ceria) CeO_2 sample.

The preparation method of the mixed oxides $Cu_6Al_{2-x}Ce_x$ with x = 0–0.8 through the LDH route is described elsewhere [41]. In brief, an appropriate amount of metal salts with the required molar ratio of Cu^{2+}/M^{3+} (M = $Al_{2-x}Ce_x$) of 3/1 was dissolved in 200 mL of an aqueous solution and dropwise added to a beaker containing 50 mL of a Na_2CO_3 solution (1 $mol{\cdot}L^{-1}$). The pH of the solution was maintained constant (10.5) by sodium hydroxide. When proceeding, the final mixture was continuously aged for 18 h in an atmospheric environment at room temperature. Then, the precipitate formed was filtered and washed with hot distilled water (60 °C) several times. The hydrotalcite solid collected was then dried in an oven for 72 h at 60 °C before grinding. Finally, the mixed oxides were obtained by the calcination of the LDH at 500 °C for 4 h.

The properties of the mixed oxides obtained through the LDH method were compared using other methodologies. Different oxides were prepared with the same molar ratio of

the $Cu_6Al_{1.2}Ce_{0.8}$ sample. The CuO-Al_2O_3-CeO_2 catalyst was prepared by the calcination of the physically mixed prepared CeO_2 with the as-received, commercial CuO and Al_2O_3. The individual metal oxide precursors were well mixed and treated for 4 h at 500 °C.

On the other hand, a sample of $(Cu_6Al_2 + CeO_2)_{500}$ was obtained by mechanically mixing the Cu_6Al_2 sample with an appropriate amount of CeO_2. The mixed oxides then also calcined at the same conditions. Finally, the as-prepared Cu_6Al_2-HT material precursor of Cu_6Al_2, with a desired amount of $Ce(NO_3)_3$, was mechanically mixed and grinded and then treated by heating under air flow at 500 °C to obtain the finally labelled $(Cu_6Al_2$-HT + $Ce(NO_3)_3)_{500}$ catalyst.

3.3. Catalyst Characterization

The real metal proportions on the sample were analyzed using inductively coupled plasma-optical emission spectroscopy (ICP-OES, iCAP-6300-DUO, Thermo Electron (Thermo Fisher Scientific, Illkirch, France). The metal oxide was dissolved in aqua regal under a microwave for 30 min and then diluted extensively before the analysis.

The XRD analysis of the crystalline structure was carried out at room temperature with a Bruker D8 Advance diffractometer (Bruker AXS, Billerica, MA, USA) equipped with a LynxEye Detector and Cu anode (λ = 1.5406 Å). The scattering intensities were obtained by a continuous scan mode at an angular range from 10 to 80º using a 0.02° step-size and a count time of 4 s per step. For each pattern, structural determination was performed by comparison with the "Joint Committee on Powder Diffraction Standards" (JCPDS) files.

The Scherrer equation was applied using the signals corresponding to the (111) of CeO_2 and (11-3) of CuO planes (Equation (1)) to estimate the size of the presented crystalline oxide phases:

$$Lc = \frac{K\,\lambda}{\beta \cos\theta} \quad (1)$$

λ = 1.1506Å, K = 0.9, θ is the peak position of the detected plan and β is the full width at half maximum (FWHM) of the peak plane θ position.

The catalysts' textural properties were obtained by nitrogen physisorption conducted on QSurf M1 apparatus thermoelectron equipment (Thermo Fisher Scientific, Illkirch, France). Prior to the N_2 molecule being adsorbed, the sample was degassed at 300 °C under vacuum before cleaning the surface, and the pressure remained constant. The specific surface area was calculated from the N_2 adsorption–desorption at −196 °C using the Brunauer–Emmett–Teller (BET) equation [58,59].

The temperature reduction of the catalytic materials was identified by means of a temperature-programmed reduction (H_2-TPR) performed using an AMI-200 instrument (ZETON ALTAMIRA, Cumming, GA, USA). In total, 30 mg of the catalyst emerged in a U-shaped quartz tube reactor. The catalyst was first pretreated at 250 °C for 2 h using pure Argon at a flow rate of 30 mL·min^{-1} to remove water adsorbed on the catalyst surface. The steam outlet from the reactor was connected to the thermal conductivity detector (TCD) for H_2 analysis. After surface cleaning, the temperature of the reactor was cooled down, and then the gas was switched to 5% v/v H_2/Ar with a 20 mL·min^{-1} constant flow rate and kept constant until the detector indicated a stable baseline. The sample was then heated from room temperature to 400 °C under the same flow (5 °C·min^{-1}), and simultaneously, the hydrogen uptake behavior profile of the sample was registered and analyzed.

TGA-DTG thermogravimetries analysis was performed under the presence of synthetic air from ambient temperature to 1000 °C (5 °C·min^{-1} ramp) in SDT Q600 (TA Instruments, New Castle, DE, USA) equipment.

3.4. Catalytic Tests

The catalytic toluene and/or CO oxidation tests were carried out in a U-shaped quartz continuous flow reactor at atmospheric pressure with 100 mg of a fixed-bed catalyst. Before the experiment, the sample was activated in the presence of air flow (2 L·h^{-1}) at 500 °C for 2 h. After pretreatment, a 100 mL·min^{-1} reactive gas flow (1000 ppm of C_7H_8 and

20% O_2 balanced by helium) was adjusted by a Michell apparatus consisting of a saturator and mass flow controllers. After stabilization, the total gas flow was passed through the catalyst bed reactor, the temperature was increased from room temperature to 400 °C (1 °C·min^{-1}), and simultaneously, the quantitative analysis started to be carried out. The resulting gas mixture was analyzed online by an agilent 490 Micro gas chromatography (Agilent Technologies Inc., Santa Clara, CA, USA) for toluene quantification and an infrared analyzer 4400 IR (ADEV, Cesano Maderno, Italia) for CO and CO_2.

Toluene conversion was calculated as a function of the carbon number for each compound of the reaction [39].

$$X_{Tol}^{T}(\%) = 100 \times \left(\frac{\left(CO_{2}{}_{Ana}^{T} - CO_{2}{}_{CO}^{T}\right) + 6 \times C_6H_{6,T}}{\left(CO_{2}{}_{Ana}^{T} - CO_{2}{}_{CO}^{T}\right) + 6 \times C_6H_{6,T} + 7 \times C_7H_{8,T}} \right) \quad (2)$$

where

X_{Tol}^{T}: toluene conversion at temperature T;
$C_6H_{6,T}$: analyzed benzene concentration at temperature T;
$\left(CO_{2}{}_{Ana}^{T} - CO_{2}{}_{CO}^{T}\right)$: CO_2 concentration produced from toluene by the following equation:

$$CO_{2}{}_{CO}^{T} = CO_{converted} = (CO_0 - CO_{Ana}^{T}) \quad (3)$$

where

$CO_{converted}$: CO converted at temperature T;
CO_0: initial inlet concentration of CO;
CO_{Ana}^{T}: obtained CO concentration at temperature T by the infrared analyzer;
$CO_{2}{}_{CO}^{T}$ refers to the detected concentrations of CO_2 produced from CO.

The CO conversion was calculated based on the ppm concentration indicated by the infrared analyzer using Equation (4).

$$X_{CO}^{T}(\%) = 100 \times \frac{\left(CO_0 - CO_{Ana}^{T}\right)}{CO_0} \quad (4)$$

4. Conclusions

The synthesis method affects the distribution of active sites in the mixed oxides. Mixed oxides derived from LDH result in highly dispersed small crystallites. The presence of Ce in the LDH seems to narrow the CuO phase size of the final obtained mixed oxides. The cerium active sites in the mixed oxides not only increase the reducibility of the materials but also create an interesting new redox couple.

Toluene oxidation over CuAlCe-based mixed oxides is related mainly to the number of different oxygen vacancies. However, the conversion of CO to CO_2 is linked directly to the presence of oxygen lattice mobility, where the CuO is the active center. CO inhibition in toluene/CO mixture co-oxidation is attributed to the competing adsorption of the molecule but also to the active site's saturation and the redox cycle ignition. Consequently, the Cu/Ce fraction in the final oxide-derived LDH preferentially influences catalyst properties and can highly alter the CO oxidation in mixtures. CuAlCe mixed oxides derived from LDH make the CO poisoning of toluene oxidation insignificant.

Within all series, the superior catalytic performance of toluene and/or CO oxidation is achieved by the $Cu_6Al_{1.2}Ce_{0.8}$ sample due to a distinguished diversity of active centers, such as a good crystallite shape and specific area and a great Cu/Ce synergy. The best operated mixed oxide is stable and maintains toluene oxidation with a high concentration of CO in the mixture stream during four cycles of reutilization. Thus, the material $Cu_6Al_{1.2}Ce_{0.8}$ appears to be a promising catalyst for application in the treatment of pollutants issued from biomass combustion.

Supplementary Materials: The following supporting information can be downloaded at: https://www.mdpi.com/article/10.3390/catal14070455/s1, Table S1: Metal composition of the mixed oxides catalysts, Table S2: Calculated H_2-TPR parameters of the prepared mixed oxides. Table S3: Temperatures corresponding to the 10%, 50% and 90% conversion of simple toluene oxidation. Table S4: Temperatures corresponding to the 10%, 50% and 90% conversion of simple CO oxidation. Table S5: Temperatures corresponding to the half conversion of toluene and CO in simple and mixture oxidation. Table S6: Temperature corresponding to the half conversion of toluene and CO in simple and mixture oxidation over $Cu_6Al_{2-x}Ce_x$ (x = 0–0.8) catalysts. Table S7: Calculated structural and textural parameters of $Cu_6Al_{2-x}Ce_x$ catalysts series. Figure S1: JPCDS cards of the obtained phases for the prepared mixed oxides. Figure S2: TGA-DSC of the raw and reused $Cu_6Al_{1.2}Ce_{0.8}$ catalyst.

Author Contributions: Conceptualization: C.E.B., S.S. and R.C.; formal analysis: C.P. (Caroline Paris) and H.D.; investigation: C.P. (Caroline Paris), H.D., C.E.B., E.G., C.P. (Christophe Poupin), S.S. and R.C.; writing—original draft preparation: C.E.B. and R.C.; writing—review and editing: C.P. (Christophe Poupin), H.D., C.E.B., E.G., C.P. (Caroline Paris), S.S. and R.C.; supervision, S.S. and R.C. All authors have read and agreed to the published version of the manuscript.

Funding: The authors gratefully acknowledge the financial support from the CPER-ECRIN program, the Hauts-de-France region and the European Community (Interreg V France-Wallonie-Vlaanderen project, "DepollutAir" (No. 1.1.18)).

Data Availability Statement: The data that support the findings of this study are available from the corresponding author upon reasonable request.

Acknowledgments: C. Paris and H. Dib thank the Région Hauts-de-France, the ULCO and the Pôle Métropolitain de la Côte d'Opale for their Ph.D. grants.

Conflicts of Interest: The authors declare no conflicts of interest.

References

1. Ozgen, S.; Cernuschi, S.; Caserini, S. An overview of nitrogen oxides emissions from biomass combustion for domestic heat production. *Renew. Sustain. Energy Rev.* **2021**, *135*, 110113. [CrossRef]
2. Lim, M.T.; Phan, A.; Roddy, D.; Harvey, A. Technologies for measurement and mitigation of particulate emissions from domestic combustion of biomass: A review. *Renew. Sustain. Energy Rev.* **2015**, *49*, 574–584. [CrossRef]
3. González, J.F.; González-Garcı, C.M.; Ramiro, A.; González, J.; Sabio, E.; Gañán, J.; Rodrı, M.A. Combustion optimisation of biomass residue pellets for domestic heating with a mural boiler. *Biomass Bioenergy* **2004**, *27*, 145–154. [CrossRef]
4. Yang, C.; Kwon, H.; Bang, B.; Jeong, S.; Lee, U. Role of biomass as low-carbon energy source in the era of net zero emissions. *Fuel* **2022**, *328*, 125206. [CrossRef]
5. Ross, A.B.; Jones, J.M.; Chaiklangmuang, S.; Pourkashanian, M.; Williams, A.; Kubica, K.; Andersson, J.T.; Kerst, M.; Danihelka, P.; Bartle, K.D. Measurement and prediction of the emission of pollutants from the combustion of coal and biomass in a fixed bed furnace. *Fuel* **2002**, *81*, 571–582. [CrossRef]
6. Sun, J.; Shen, Z.; Zhang, L.; Zhang, Y.; Zhang, T.; Lei, Y.; Niu, X.; Zhang, Q.; Dang, W.; Han, W.; et al. Volatile organic compounds emissions from traditional and clean domestic heating appliances in Guanzhong Plain, China: Emission factors, source profiles, and effects on regional air quality. *Environ. Int.* **2019**, *133*, 105252. [CrossRef] [PubMed]
7. Maxwell, D.; Gudka, B.A.; Jones, J.M.; Williams, A. Emissions from the combustion of torrefied and raw biomass fuels in a domestic heating stove. *Fuel Process. Technol.* **2020**, *199*, 106266. [CrossRef]
8. He, C.; Cheng, J.; Zhang, X.; Douthwaite, M.; Pattisson, S.; Hao, Z. Recent Advances in the Catalytic Oxidation of Volatile Organic Compounds: A Review Based on Pollutant Sorts and Sources. *Chem. Rev.* **2019**, *119*, 4471–4568. [CrossRef] [PubMed]
9. Zhang, H.; Zhang, X.; Wang, Y.; Bai, P.; Hayakawa, K.; Zhang, L.; Tang, N. Characteristics and Influencing Factors of Polycyclic Aromatic Hydrocarbons Emitted from Open Burning and Stove Burning of Biomass: A Brief Review. *Int. J. Environ. Res. Public Health* **2022**, *19*, 3944. [CrossRef] [PubMed]
10. Brummer, V.; Teng, S.Y.; Jecha, D.; Skryja, P.; Vavrcikova, V.; Stehlik, P. Contribution to cleaner production from the point of view of VOC emissions abatement: A review. *J. Clean. Prod.* **2022**, *361*, 132112. [CrossRef]
11. Genty, E.; Cousin, R.; Capelle, S.; Gennequin, C.; Siffert, S. Catalytic Oxidation of Toluene and CO over Nanocatalysts Derived from Hydrotalcite-Like Compounds ($X_6^{2+}Al_2^{3+}$): Effect of the Bivalent Cation. *Eur. J. Inorg. Chem.* **2012**, *2012*, 2802–2811. [CrossRef]
12. El Khawaja, R.; Veerapandian, S.K.P.; Bitar, R.; De Geyter, N.; Morent, R.; Heymans, N.; De Weireld, G.; Barakat, T.; Ding, Y.; Abdallah, G.; et al. Boosting VOCs elimination by coupling different techniques. *Chem. Synth.* **2022**, *2*, 13. [CrossRef]
13. Yang, C.; Miao, G.; Pi, Y.; Xia, Q.; Wu, J.; Li, Z.; Xiao, J. Abatement of various types of VOCs by adsorption/catalytic oxidation: A review. *Chem. Eng. J.* **2019**, *370*, 1128–1153. [CrossRef]

14. Gong, P.; He, F.; Xie, J.; Fang, D. Catalytic removal of toluene using MnO_2-based catalysts: A review. *Chemosphere* **2023**, *318*, 137938. [CrossRef] [PubMed]
15. Zhang, Y.; Li, C.; Zhu, Y.; Du, X.; Lyu, Y.; Li, S.; Zhai, Y. Insight into the enhanced performance of toluene removal from simulated flue gas over Mn-Cu oxides modified activated coke. *Fuel* **2020**, *276*, 118099. [CrossRef]
16. Wang, Q.; Li, Y.; Serrano-Lotina, A.; Han, W.; Portela, R.; Wang, R.; Bañares, M.A.; Yeung, K.L. Operando Investigation of Toluene Oxidation over 1D Pt@CeO_2 Derived from Pt Cluster-Containing MOF. *J. Am. Chem. Soc.* **2021**, *143*, 196–205. [CrossRef] [PubMed]
17. Guo, Y.; Wen, M.; Li, G.; An, T. Recent advances in VOC elimination by catalytic oxidation technology onto various nanoparticles catalysts: A critical review. *Appl. Catal. B Environ.* **2021**, *281*, 119447. [CrossRef]
18. Scirè, S.; Liotta, L.F. supported gold catalysts for the total oxidation of volatile organic compounds. *Appl. Catal. B Environ.* **2012**, *125*, 222–246. [CrossRef]
19. Liotta, L.F. Catalytic oxidation of volatile organic compounds on supported noble metals. *Appl. Catal. B Environ.* **2010**, *100*, 403–412. [CrossRef]
20. Zhang, L.; Xue, L.; Lin, B.; Zhao, Q.; Wan, S.; Wang, Y.; Jia, H.; Xiong, H. Noble Metal Single-Atom Catalysts for the Catalytic Oxidation of Volatile Organic Compounds. *ChemSusChem* **2022**, *15*, e202102494. [CrossRef]
21. Zhang, Z.; Jiang, Z.; Shangguan, W. Low-temperature catalysis for VOCs removal in technology and application: A state-of-the-art review. *Catal. Today* **2016**, *264*, 270–278. [CrossRef]
22. Bao, L.; Zhu, S.; Chen, Y.; Wang, Y.; Meng, W.; Xu, S.; Lin, Z.; Li, X.; Sun, M.; Guo, L. Anionic defects engineering of Co_3O_4 catalyst for toluene oxidation. *Fuel* **2022**, *314*, 122774. [CrossRef]
23. Zhang, J.; Zhang, L.; Cheng, Y.; Liu, Y. Construction of oxygen vacancies in δ-MnO_2 for promoting low-temperature toluene oxidation. *Fuel* **2023**, *332*, 126104. [CrossRef]
24. Carabineiro, S.A.C.; Chen, X.; Konsolakis, M.; Psarras, A.C.; Tavares, P.B.; Órfão, J.J.M.; Pereira, M.F.R.; Figueiredo, J.L. Catalytic oxidation of toluene on Ce–Co and La–Co mixed oxides synthesized by exotemplating and evaporation methods. *Catal. Today* **2015**, *244*, 161–171. [CrossRef]
25. Wang, Y.; Yang, D.; Li, S.; Zhang, L.; Zheng, G.; Guo, L. Layered copper manganese oxide for the efficient catalytic CO and VOCs oxidation. *Chem. Eng. J.* **2019**, *357*, 258–268. [CrossRef]
26. Kamal, M.S.; Razzak, S.A.; Hossain, M.M. Catalytic oxidation of volatile organic compounds (VOCs)—A review. *Atmos. Environ.* **2016**, *140*, 117–134. [CrossRef]
27. Murindababisha, D.; Yusuf, A.; Sun, Y.; Wang, C.; Ren, Y.; Lv, J.; Xiao, H.; Chen, G.Z.; He, J. Current progress on catalytic oxidation of toluene: A review. *Environ. Sci. Pollut. Res.* **2021**, *28*, 62030–62060. [CrossRef] [PubMed]
28. Li, B.; Xiong, H.; Dai, W.; Huang, Z.; Zhong, X.; Zhang, J.; Zhou, L.; Wu, K.; Zou, J.; Luo, X. Enabling the activation of lattice oxygen and high distribution of Co^{3+} on $LaCoO_3$ surface through fluorine incorporation to promote toluene combustion. *Appl. Catal. B Environ. Energy* **2024**, *347*, 123828. [CrossRef]
29. Zheng, Y.; Xu, W.; Yang, J.; Shan, C.; Wang, Y.; Han, R.; Zang, G.; Liu, Q. Catalytic oxidation of VOCs and CO on cobalt-based Materials: Strategies and mechanisms for improving activity and stability. *Chem. Eng. J.* **2024**, *484*, 149296. [CrossRef]
30. Cheng, G.; Song, Z.; Mao, Y.; Zhang, J.; Wang, K.; Li, H.; Huang, Z. Effect of Ce_2O_3 phase transition on the catalytic oxidation for toluene over CeO_2 catalysts. *Fuel* **2024**, *368*, 131641. [CrossRef]
31. Zhao, L.; Huang, Y.; Zhang, J.; Jiang, L.; Wang, Y. Al_2O_3-modified CuO-CeO_2 catalyst for simultaneous removal of NO and toluene at wide temperature range. *Chem. Eng. J.* **2020**, *397*, 125419. [CrossRef]
32. Pérez, A.; Molina, R.; Moreno, S. Enhanced VOC oxidation over Ce/CoMgAl mixed oxides using a reconstruction method with EDTA precursors. *Appl. Catal. A Gen.* **2014**, *477*, 109–116. [CrossRef]
33. Ye, Z.; Giraudon, J.-M.; Nuns, N.; Simon, P.; De Geyter, N.; Morent, R.; Lamonier, J.-F. Influence of the preparation method on the activity of copper-manganese oxides for toluene total oxidation. *Appl. Catal. B Environ.* **2018**, *223*, 154–166. [CrossRef]
34. Zeng, Y.; Wang, Y.; Song, F.; Zhang, S.; Zhong, Q. The effect of CuO loading on different method prepared CeO_2 catalyst for toluene oxidation. *Sci. Total Environ.* **2020**, *712*, 135635. [CrossRef] [PubMed]
35. Du, Y.; Gao, F.; Zhou, Y.; Yi, H.; Tang, X.; Qi, Z. Recent advance of CuO-CeO_2 catalysts for catalytic elimination of CO and NO. *J. Environ. Chem. Eng.* **2021**, *9*, 106372. [CrossRef]
36. Avgouropoulos, G.; Ioannides, T.; Matralis, H. Influence of the preparation method on the performance of CuO–CeO_2 catalysts for the selective oxidation of CO. *Appl. Catal. B Environ.* **2005**, *56*, 87–93. [CrossRef]
37. Moreno-Román, E.J.; González-Cobos, J.; Guilhaume, N.; Gil, S. Toluene and 2-propanol mixture oxidation over Mn_2O_3 catalysts: Study of inhibition/promotion effects by in-situ DRIFTS. *Chem. Eng. J.* **2023**, *470*, 144114. [CrossRef]
38. Mo, S.; Zhang, Q.; Sun, Y.; Zhang, M.; Li, J.; Ren, Q.; Fu, M.; Wu, J.; Chen, L.; Ye, D. Gaseous CO and toluene co-oxidation over monolithic core–shell Co_3O_4 -based hetero-structured catalysts. *J. Mater. Chem. A* **2019**, *7*, 16197–16210. [CrossRef]
39. Bi, F.; Ma, S.; Gao, B.; Yang, Y.; Wang, L.; Fei, F.; Xu, J.; Huang, Y.; Wu, M.; Zhang, X. Non-oxide supported Pt-metal-group catalysts for efficiently CO and toluene co-oxidation: Difference in water resistance and degradation intermediates. *Fuel* **2023**, *344*, 128147. [CrossRef]
40. Kang, S.B.; Hazlett, M.; Balakotaiah, V.; Kalamaras, C.; Epling, W. Effect of Pt:Pd ratio on CO and hydrocarbon oxidation. *Appl. Catal. B Environ.* **2018**, *223*, 67–75. [CrossRef]
41. Kang, S.B.; Kalamaras, C.; Balakotaiah, V.; Epling, W. Zoning and Trapping Effects on CO and Hydrocarbon Light-Off in Diesel Oxidation Catalysts. *Ind. Eng. Chem. Res.* **2017**, *56*, 13628–13633. [CrossRef]

42. Genty, E.; Brunet, J.; Poupin, C.; Ojala, S.; Siffert, S.; Cousin, R. Influence of CO addition on the toluene total oxidation over Co based mixed oxide catalysts. *Appl. Catal. B Environ.* **2019**, *247*, 163–172. [CrossRef]
43. Genty, E.; Serhal, C.A.; El Khawaja, R.; Dib, H.; Labaki, M.; Mallard, I.; Poupin, C.; Siffert, S.; Cousin, R. Mixed Oxides Issued from Hydrotalcite Precursors for Toluene and CO Total Oxidation: Comparison of Preparation Method. *J. Nanosci. Nanotechnol.* **2020**, *20*, 1130–1139. [CrossRef]
44. Yun, J.; Wu, L.; Hao, Q.; Teng, Z.; Gao, X.; Dou, B.; Bin, F. Non-equilibrium plasma enhanced oxygen vacancies of CuO/CeO_2 nanorod catalysts for toluene oxidation. *J. Environ. Chem. Eng.* **2022**, *10*, 107847. [CrossRef]
45. Menon, U.; Poelman, H.; Bliznuk, V.; Galvita, V.V.; Poelman, D.; Marin, G.B. Nature of the active sites for the total oxidation of toluene by $CuOCeO_2/Al_2O_3$. *J. Catal.* **2012**, *295*, 91–103. [CrossRef]
46. Nakagawa, K.; Ohshima, T.; Tezuka, Y.; Katayama, M.; Katoh, M.; Sugiyama, S. Morphological effects of CeO_2 nanostructures for catalytic soot combustion of CuO/CeO_2. *Catal. Today* **2015**, *246*, 67–71. [CrossRef]
47. Zeng, Y.; Haw, K.-G.; Wang, Z.; Wang, Y.; Zhang, S.; Hongmanorom, P.; Zhong, Q.; Kawi, S. Double redox process to synthesize $CuO–CeO_2$ catalysts with strong Cu–Ce interaction for efficient toluene oxidation. *J. Hazard. Mater.* **2021**, *404*, 124088. [CrossRef]
48. Mao, L.; Song, Z.; Fan, J.; Cui, Y.; Zhang, K.; He, Q.; Zhang, R.; Wang, X. Regulating asymmetric oxygen vacancies in copper-ceria catalysts for achievement of excellent toluene catalytic oxidation. *Sep. Purif. Technol.* **2024**, *334*, 126035. [CrossRef]
49. Chen, Y.; Xue, J.; Shen, X.; Chen, J.; Quarcoo, F.H.; Rac, V.; Rakić, V.; Li, X.; Du, X. Diving into the interface-mediated Mars-van Krevelen (M−vK) characteristic of CuO_x-supported CeO_2 catalysts. *Appl. Catal. B Environ.* **2024**, *342*, 123368. [CrossRef]
50. Rawat, A.; Dhakla, S.; Lama, P.; Pal, T.K. Fixation of carbon dioxide to aryl/aromatic carboxylic acids. *J. CO_2 Util.* **2022**, *59*, 101939. [CrossRef]
51. Viinikainen, T.S.; Lehtonen, J.S. Toluene Oxidation in the Absence and Presence of CO, CO_2, Water and H_2 over ZrO_2-Based Gasification Gas Clean-Up Catalysts. *ChemistrySelect* **2017**, *2*, 1663–1670. [CrossRef]
52. Peng, P.; Li, J.; Mo, S.; Zhang, Q.; Shen, T.; Xie, Q. Bimetallic Pt-Co Nanoparticle Deposited on Alumina for Simultaneous CO and Toluene Oxidation in the Presence of Moisture. *Processes* **2021**, *9*, 230. [CrossRef]
53. Huttunen, P.K.; Labadini, D.; Asselin, G.; Hafiz, S.S.; Gokalp, S.; Kipreos, M.D.; Foster, M. DRIFTS investigation of toluene oxidation on CeO_2 nanoparticles. *Surf. Sci.* **2022**, *720*, 122042. [CrossRef]
54. Zhang, J.; Wu, K.; Xiong, J.; Ren, Q.; Zhong, J.; Cai, H.; Huang, H.; Chen, P.; Wu, J.; Chen, L.; et al. Static and dynamic quantification tracking of asymmetric oxygen vacancies in copper-ceria catalysts with superior catalytic activity. *Appl. Catal. B Environ.* **2022**, *316*, 121620. [CrossRef]
55. Sun, W.; Huang, Y.; Li, X.; Huang, Z.; Xu, H.; Shen, W. Catalytic Combustion of Toluene over Highly Dispersed Cu-CeO_x Derived from Cu-Ce-MOF by EDTA Grafting Method. *Catalysts* **2021**, *11*, 519. [CrossRef]
56. Lyu, Y.; Xu, J.; Chen, S.; Wang, S.; Liu, X. Simultaneous catalytic oxidation of toluene and CO over Cu-V/Al-Ce catalysts: Physicochemical properties-activity relationship and simultaneous oxidation mechanism. *J. Hazard. Mater.* **2024**, *466*, 133507. [CrossRef] [PubMed]
57. Dib, H.; El Khawaja, R.; Rochard, G.; Poupin, C.; Siffert, S.; Cousin, R. CuAlCe Oxides Issued from Layered Double Hydroxide Precursors for Ethanol and Toluene Total Oxidation. *Catalysts* **2020**, *10*, 870. [CrossRef]
58. Qu, Q.; Qiu, L.; Li, M.-Z.; Sun, G.-T.; Chen, H.-Y.; Guo, X.-H. Synergistic Effects of Pyrolysis Temperature, Iron Ion Concentration and Solid/Liquid Ratio on the Properties and Cr(VI) Removal Performance of Magnetic Carbon. *J. Water Process Eng.* **2023**, *53*, 103785. [CrossRef]
59. Qu, Q.; Chen, Z.; Sun, G.-T.; Qiu, L.; Zhu, M.-Q. $CoFe_2O_4$ Nanoparticles as a Bifunctional Agent on Activated Porous Carbon for Battery-Type Asymmetrical Supercapacitor. *Chem. Synth.* **2024**, *4*, 26. [CrossRef]